A comparative study on generation and propagation of nonlinear waves in shallow waters

Liu, Jiaqi; Hayatdavoodi, Masoud; Cengiz Ertekin, R.

DOI:
10.3390/jmse11050917

Publication date:
2023

Journal of *Marine Science and Engineering*

MDPI

Article

A Comparative Study on Generation and Propagation of Nonlinear Waves in Shallow Waters

Jiaqi Liu [1], Masoud Hayatdavoodi [1,2,*] and R. Cengiz Ertekin [1,3]

[1] College of Shipbuilding Engineering, Harbin Engineering University, Harbin 150001, China
[2] Civil Engineering Department, School of Science and Engineering, University of Dundee, Dundee DD1 4HN, UK
[3] Ocean & Resources Engineering Department, University of Hawaii, Honolulu, HI 96822, USA
* Correspondence: mhayatdavoodi@dundee.ac.uk; Tel.: +44-(0)1382-385720

Abstract: This study is concerned with the generation and propagation of strongly nonlinear waves in shallow water. A numerical wave flume is developed where nonlinear waves of solitary and cnoidal types are generated by use of the Level I Green-Naghdi (GN) equations by a piston-type wavemaker. Waves generated by the GN theory enter the domain where the fluid motion is governed by the Navier–Stokes equations to achieve the highest accuracy for wave propagation. The computations are performed in two dimensions, and by an open source computational fluid dynamics package, namely OpenFoam. Comparisons are made between the characteristics of the waves generated in this wave tank and by use of the GN equations and the waves generated by Boussinesq equations, Laitone's 1st and 2nd order equations, and KdV equations. We also consider a numerical wave tank where waves generated by the GN equations enter a domain in which the fluid motion is governed by the GN equations. Discussion is provided on the limitations and applicability of the GN equations in generating accurate, nonlinear, shallow-water waves. The results, including surface elevation, velocity field, and wave celerity, are compared with laboratory experiments and other theories. It is found that the nonlinear waves generated by the GN equations are highly stable and in close agreement with laboratory measurements.

Keywords: Green–Naghdi equations; Navier–Stokes equations; Boussinesq equations; KdV equation; solitary wave; cnoidal wave; numerical wave tank

Citation: Liu, J.; Hayatdavoodi, M.; Ertekin, R.C. A Comparative Study on Generation and Propagation of Nonlinear Waves in Shallow Waters. *J. Mar. Sci. Eng.* **2023**, *11*, 917. https://doi.org/10.3390/jmse11050917

Academic Editors: Helena M. Ramos, Juan Antonio Rodríguez Díaz, Jorge Matos and Lev Shemer

Received: 25 March 2023
Revised: 18 April 2023
Accepted: 19 April 2023
Published: 25 April 2023

1. Introduction

Solitary wave is a nonlinear wave with an isolated elevation of finite amplitude and permanent form over a flat seafloor. The presence of the solitary wave was first reported by [1], who conducted extensive experiments on the generation and propagation of the wave in 1834 and 1835, see [2]. At the time, there was a conflict between Russell's observations and [3] prediction (shallow-water-theory) that a wave of finite amplitude cannot propagate without a change of form. This conflict was resolved independently by [4–8]. Boussinesq and Rayleigh showed that appropriate allowance for vertical acceleration and finite amplitude leads to an explicit solution of the solitary wave. Ref. [6]'s theory of solitary wave was accepted although the solution is only first-order accurate. Ref. [9] suggested a theoretical solution whose mathematical formulations are provided by Lee et al. (1982). As [9]'s equations are implicit, an iterative method, such as Newton–Raphson, is needed to solve the equations. An equation only admitting right-running solutions was derived by [10], named the Korteweg–de Vries (KdV) equation.

The periodic form of a solitary wave with the same height is named a cnoidal wave by [7]. A cnoidal wave is a periodic wave with isolated wave crests and flat wave troughs. A cnoidal wave without a nonlinear and asymmetrical wave profile about the still-water level (SWL) could become a sinusoidal wave. Ref. [10] obtained the solutions for cnoidal waves by means of the Jacobian elliptic cosine function Cn contained in the wave profile

formula. Following the idea of [10] about cnoidal waves, Ref. [11] established the Keulegan–Patterson theory for cnoidal waves. Ref. [12] proved the existence of cnoidal waves with a complex potential function. By then, the equations were complicated to be used in practical application for the incompleteness of second-order solutions. Based on the work of [13,14] a second-order approximation to the cnoidal wave theory was developed by using the expansion method, and [15] added a nonzero term to the equations.

Ref. [16] developed the Green–Naghdi (GN) equations for shallow-water wave motions based on the directed fluid sheet theory. The GN theory satisfies exactly the nonlinear boundary conditions and conservation of mass, postulates the integrated form of the conservation of momentum, and does not require the irrotationality of the flow. This set of equations contains solutions for solitary wave (see [17]) and cnoidal wave (see [18]). The GN equations are used successfully for a wide range of problems involving water wave dynamics; for example, nonlinear wave scattering by submerged objects ([19]), and diffraction and refraction of solitary and cnoidal waves ([20]).

Although there are several equations that can be used to describe the solitary and cnoidal waves, it is difficult to solve the equations analytically due to the nonlinear nature of these waves, especially the implicit part of solutions of the cnoidal wave, see [18]. Thanks to the increase in computational power, the computational fluid dynamics (CFD) approach is used in the study of solitary and cnoidal waves. The waves are generated by use of different equations, see, e.g., Ref. [21,22] for the use of the KdV equations to generate solitary waves, Ref. [23] for the use of the GN equations to generate solitary waves, and propagate in the domain governed by the Navier–Stokes (NS) equations, Ref. [24] for the use of cnoidal waves by use of the GN equations, and [25] for the use of the Boussinesq equations to generate solitary waves. It is desirable to generate accurate nonlinear waves when studying wave dynamics in coastal zones, for example for wave propagation over an uneven seafloor, or in wave-structure interaction problems. While various theories are used to generate nonlinear waves of solitary and cnoidal types in computational wave tanks, there has not been any systematic investigation about the accuracy and stability of the waves when compared to each other. It is desirable to find out how the solitary wave and cnoidal wave generated based on the existing equations propagate in the computational fluid dynamics-based numerical wave tanks.

In this study, we create a numerical tank to investigate the accuracy and stability of solitary and cnoidal waves of different theories. We develop numerical wave makers capable of generating solitary and cnoidal waves of different theories. Waves are generated by a piston-type wave maker and enter a domain of constant water depth, where the flow is governed by the NS equations. We then investigate the characteristic of the solitary and cnoidal waves of different theories within the domain, and compare the results with available laboratory measurements. To further assess the performance of the GN equations, we also create a numerical wave tank based entirely on the GN equations, i.e., the waves generated by the GN theory enter a domain where the flow is governed by the GN equations. The results are then compared with the laboratory measurements, and with the results of the case of the NS domain.

In this paper, we first present the theories used for wave generation and propagation, followed by the introduction of the set-up of the numerical tank. Steady-state results are given first and unsteady results of solitary waves and cnoidal waves are presented and discussed thereafter. The conclusions then follow.

2. The Theories and Numerical Set Up

We create a numerical tank, in which solitary and cnoidal waves generated by different theories are investigated. The governing equations of the domain and the wave theories used are described in this section.

We adopt a right-handed two-dimensional (2D) Cartesian coordinate system, with x_1 pointing to the right, and x_2 pointing vertically opposite to the direction of the gravitational acceleration such that $x_2 = 0$ is the SWL. Indicial notation and Einstein's summation

convention are used. Subscripts after the comma indicate differentiation. The equations are given in dimensionless forms using density of water, ρ, gravitational acceleration, g, and water depth, h, as a dimensionally independent set. Hence, the dimensionless form of time is $t' = t \times \sqrt{g/h}$, surface elevation is $\eta' = \eta/h$, velocity is $u' = u/\sqrt{gh}$ and pressure is $p' = p/\rho gh$. For simplicity, we drop primes from all dimensionless variables in the rest of this work unless otherwise indicated.

2.1. The Navier-Stokes Equations

For a homogeneous, Newtonian and incompressible fluid, the 2D NS equations are given by the following conservation of mass and momentum equations:

$$u_{i,i} = 0, \quad i = 1,2 \tag{1}$$

$$u_{j,t} + (u_i u_j)_{,i} = \frac{1}{Fr^2} g_j - p_{,j} + \frac{1}{Re} u_{j,ii}, \quad i,j = 1,2 \tag{2}$$

where $\vec{u} = u_i \vec{e_i}$ is the velocity vector, and $\vec{e_i}$ is the unit normal vector in the i-th direction, $Fr = \frac{U}{\sqrt{gl}}$ is the Froude number, with U and l as the characteristic velocity and length, respectively, $Re = \frac{Ul}{\nu}$ is the Reynolds number, ν is kinematic viscosity, $\vec{g} = (0, -1)$ is the gravitational acceleration vector, and p is the pressure.

A computational tank is created, in which waves are generated by the use of different wave theories and propagate over a flat tank floor. A schematic of the tank is shown in Figure 1. The tank is separated by dash lines into three parts, namely the wave generation zone, the computational domain and the wave absorption zone. Within the computational domain, the governing equations are solved for both water and air above. The volume of fluid method, originally introduced by [26], is used to determine the free surface between air and water.

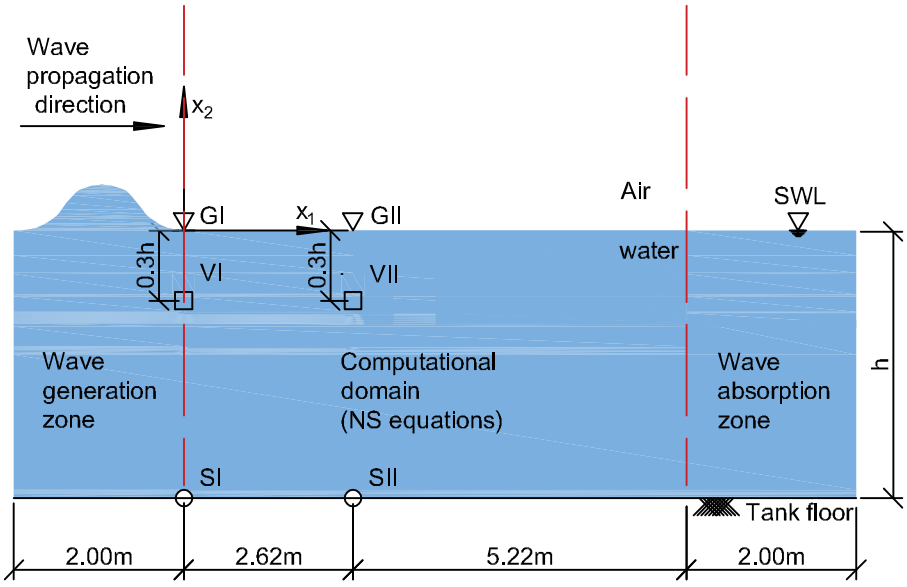

Figure 1. Schematic of the NS computational domain used in this study. Solitary and cnoidal waves are created at the generation zone, using different theories.

The Finite Volume approach is used to discretize the equations. The boundary conditions used in this study are the same as that of [27]. The details of these boundary conditions can be found in, e.g., [28,29].

2.2. The Green–Naghdi Equations

Considering the theory of directed fluid sheets of an incompressible fluid and from the laws of conservation of mass and linear momentum, [30] derived a set of equations, the Green–Naghdi (GN) equations, describing the nonlinear motion of inviscid fluids. The dimensionless GN equations read as

$$\eta_{,t} + [(1+\eta-\alpha)u_1]_{,1} = \alpha_{,t}, \tag{3}$$

$$\dot{u}_1 + \eta_{,1} + \hat{p}_{,1} = -\frac{1}{6}[2\eta+\alpha]_{,1}\ddot{\alpha} + [4\eta-\alpha]_{,1}\ddot{\eta} + (1+\eta-\alpha)[\ddot{\alpha}+2\ddot{\eta}]_{,1}, \tag{4}$$

$$u_2 = \dot{\alpha} + \frac{x_2+1-\alpha}{\eta+1-\alpha}(\dot{\eta}-\dot{\alpha}), \tag{5}$$

$$\bar{p} = \frac{1}{2}(1+\eta-\alpha)(\ddot{\alpha}+\ddot{\eta}+2) + \hat{p}, \tag{6}$$

where η is the free surface elevation measured from the SWL, $\alpha(x_1,t)$ describes the bottom surface of the fluid sheet measured from a fixed reference point, $\bar{p}(x_1,t)$ is the pressure on α, and $\hat{p}(x_1,t)$ is the pressure on top of the fluid sheet. The superposed dot denotes the material time derivative, and double dot is the second material derivative.

The pressure distribution in shallow water, p, is given as ([31,32]),

$$p(x_1,x_2,t) = \frac{1}{2}(1+\eta-x_2)(\ddot{\alpha}+\ddot{\eta}+2) + \hat{p}. \tag{7}$$

In the cases studied here, the bottom surface is flat and stationary, hence $\alpha = 0$ and $\ddot{\alpha} = 0$, and we assume $\hat{p} = 0$, i.e., pressure is atmospheric on the top surface. Hence, Equations (5) and (7) can be written as,

$$u_2(x_1,x_2,t) = \frac{x_2+1}{\eta+1}\dot{\eta}, \tag{8}$$

and

$$p(x_1,x_2,t) = \frac{1}{2}(1+\eta-x_2)(\ddot{\eta}+2). \tag{9}$$

The above solution belongs to the Level I GN equations, in which the vertical velocity varies linearly along the water column and horizontal velocity is invariant in the vertical direction. The Level I GN equations, hence, are best applicable to the propagation of long waves in shallow water. High level GN equations can be obtained by considering higher order functions for the distribution of the velocities in the vertical direction, see, e.g., [33,34].

2.3. Solitary Wave Solution

The solitary wave surface elevation of the Level I GN equations is given by [16] as

$$\eta(x_1,t) = A\ sech^2(\epsilon x_{C1}), \tag{10}$$

where A is the amplitude of the solitary wave, $x_{C1} = (x_1 - Ct)$, $\epsilon = \sqrt{\frac{3A}{4(A+1)}}$, and C is the wave speed, which is

$$C = \sqrt{(A+1)}. \tag{11}$$

The horizontal particle velocity is given by

$$u_1(x_1,t) = C\frac{\eta}{1+\eta}. \tag{12}$$

Equations (8)–(10) can be used to obtain analytical solutions for the solitary wave velocity and pressure fields. $\dot{\eta}$ is given by

$$\dot{\eta} = \eta_{,t} + u_1\eta_{,1} + u_2\eta_{,2}. \tag{13}$$

The first part of the right-hand side of Equation (13) is obtained as

$$\eta_{,t} = [A\ sech^2(\epsilon x_{C1})]_{,t} = 2A\epsilon C\ cosh^{-2}(\epsilon x_{C1})tanh(\epsilon x_{C1}), \tag{14}$$

The second part of the right-hand side of Equation (13) is given as

$$u_1\eta_{,1} = u_1[A\ sech^2(\epsilon x_{C1})]_{,1} = -2u_1A\epsilon\ cosh^{-2}(\epsilon x_{C1})\ tanh(\epsilon x_{C1}). \tag{15}$$

As $\eta(x_1, t)$ is a function of x_1 and t, but not x_2, the third part on the right-hand side of Equation (13) is given as

$$u_2\eta_{,2} = u_2[A\ sech^2(\epsilon x_{C1})]_{,2} = 0. \tag{16}$$

Substituting Equations (14)–(16) into Equation (13) gives

$$\dot{\eta} = 2A\epsilon(C - u_1)\ sech^2(\epsilon x_{C1})\ tanh(\epsilon x_{C1}), \tag{17}$$

and, substituting Equation (17) into Equation (8) gives

$$u_2(x_1, x_2, t) = 2\frac{x_2 + 1}{\eta + 1}\epsilon\eta\ tanh(\epsilon x_{C1})(C - u_1). \tag{18}$$

Next, we obtain $\ddot{\eta}$, given as

$$\ddot{\eta} = \dot{\eta}_{,t} + u_1\dot{\eta}_{,1} + u_2\dot{\eta}_{,2}. \tag{19}$$

For the first part of the right-hand side of Equation (19), we can write

$$\dot{\eta}_{,t} = 2A\epsilon^2(C - u_1)C(3\ sech^2(\epsilon x_{C1})\ tanh^2(\epsilon x_{C1}) - 1). \tag{20}$$

For the second part of the right-hand side of Equation (19)

$$u_1\dot{\eta}_{,1} = -2A\epsilon^2(C - u_1)u_1(3\ sech^2(\epsilon x_{C1})\ tanh^2(\epsilon x_{C1}) - 1). \tag{21}$$

As in the derivation of Equation (16), $\eta(x_1, t)$ is a function of x_1 and t, but not x_2; therefore, the third part of the right-side of Equation (19) can be written as

$$u_2\dot{\eta}_{,2} = 0. \tag{22}$$

Hence, substituting Equations (20)–(22) into Equation (19) gives

$$\ddot{\eta} = 2A\epsilon^2(C - u_1)^2(3\ sech^2(\epsilon x_{C1})\ tanh^2(\epsilon x_{C1}) - 1), \tag{23}$$

Substituting Equation (23) into Equation (7) gives

$$p(x_1, x_2, t) = (\eta - x_2)(2A\epsilon^2(C - u_1)^2(3\ sech^2(\epsilon x_{C1})\ tanh^2(\epsilon x_{C1}) - 1) + 1). \tag{24}$$

Equations (10), (12), (18) and (24) provide the surface elevation, horizontal and vertical velocities and the pressure under a steady-state solitary wave solution of the GN equations.

There are several solutions of a solitary wave provided by, e.g., Boussinesq (1872), [14] and KdV equations given by [10]. The analytical solutions (used in this study) and the GN solution derived above are listed in Table 1.

Table 1. Solutions of solitary wave by different theories.

	Boussinesq	**KdV**	**Laitone's 1st Order**	**Laitone's 2nd Order**	**GN**
η	$A\ sech^2(\epsilon_{BL}x_{C1})$	$A\ sech^2(\epsilon_{BL}x_{C1})$	$Asech^2(\epsilon_{BL}x_{C1})$	$A\ sech^2\chi_2$ $-3A^2\ sech^2\chi_2$ $\times(1-\ sech^2\chi_2)/4$	$A\ sesh^2(\epsilon x_{C1})$
C	$\sqrt{1+A}$	$\sqrt{1+A}$	$\sqrt{1+A/2}$	$\sqrt{1+A/2-3A^2/20}$	$\sqrt{1+A}$
u_1	$C\eta/(1+\eta)$	$A[a_{KdV}$ $+b_{KdV}$ $\times cosh(\sqrt{3A}x_{C1})]$ $\times sech^4(\epsilon_{BL}x_{C1})/4$	$A\ sech^2(\epsilon_{BL}x_{C1})$	$A(1+A/4-3Ax_2^2/2)$ $\times sech^2\chi_2$ $+\epsilon_{L1}\ sech^4\chi_2$	$C\eta/(1+\eta)$
u_2		$\sqrt{3A^3}(1+x_2)$ $\times[c_{KdV}+d_{KdV}$ $\times cosh(\sqrt{3A}x_{C1})]$ $\times sech(\epsilon_{BL}x_{C1})/4$	κx_2 $\times sech^2\chi$ $\times tanh\chi$	$\kappa(x_2+1)\ sech^2\chi_2$ $\times tanh[(1-3A/8)\chi_2]$ $-Ax_2^2/2+A\ tan\epsilon_{L2}$ $\times sech^2\chi_2$	$2\epsilon\eta$ $\times tanh(\epsilon x_{C1})$ $\times(C-u_1)$ $\times(x_2+1)$ $/(\eta+1)$

where $\epsilon=\sqrt{3A/4(A+1)}$, $\epsilon_{BL}=\sqrt{3A/4}$, $\kappa=\sqrt{3A^3}$, $\chi=\sqrt{3/4}x_{C1}$, $\chi_2=x_1\sqrt{3A/(4(1-5A/8)}-Ct$, $\epsilon_{L1}=A^2(-1+9x_2^2/4)$, $\epsilon_{L2}=-2+3x_2^2$, $a_{KdV}=2+A+12Ax_2+6Ax_2^2$, $b_{KdV}=2-A-6Ax_2-3Ax_2^2$, $c_{KdV}=2-7A+10Ax_2+5Ax_2^2$, $d_{KdV}=2+A-2Ax_2-Ax_2^2$.

2.4. Cnoidal Wave Solution

Similar to the solitary wave, there are several solutions for the cnoidal wave, such as through the Boussinesq equations, KP equations and KdV equation. The cnoidal waves generated according to the GN equations, KP equations, and KdV equation are discussed in this study.

2.4.1. The Green-Naghdi Equations

The cnoidal wave solution of the GN equations provided by [18] gives the water surface elevation, the wave phase speed, C, and the water particle velocity as

$$C^2=(1+\eta_1)(1+\eta_2)(1+\eta_3), \tag{25}$$

where $\eta_1=\frac{H}{k^2}(1-\frac{E}{K})$, $\eta_2=\frac{H}{k^2}(1-k^2-\frac{E}{K})$, and $\eta_3=\frac{H}{k^2}\frac{E}{K}$ are three wave parameters,

$$\eta=\eta_2+HC_n^2=\frac{H}{k^2}(1-k^2-\frac{E}{K})+HC_n^2, \tag{26}$$

$$u_1=\frac{\eta}{1+\eta}C, \tag{27}$$

$$u_2=\frac{1+x_2}{(1+\eta)}\frac{\partial\eta}{\partial x_1}C, \tag{28}$$

where H is the wave height of the cnoidal wave, K is the complete elliptic integral of the first kind, E is the complete elliptic integral of the second kind, C_n is the Jacobian elliptic function and k is the modulus of the respective elliptic integral function. For details, see [18].

2.4.2. The Keulegan and Patterson Equations

The solution of cnoidal wave derived by [11] share Equations (25) and (26) for C and η with the solution of the GN theory. The equations for u_1 and u_2 are:

$$u_1=(\eta-\frac{1}{4}\eta^2+(\frac{1}{3}-\frac{1}{2}(1+x_2)^2)\frac{\partial^2\eta}{\partial x_1^2})C, \tag{29}$$

$$u_2=-(1+x_2)((1-\frac{1}{2}\eta)\frac{\partial\eta}{\partial x_1}+\frac{1}{3}(1+\frac{1}{2}(1+x_2)^2)\frac{\partial^3\eta}{\partial x_1^3})C. \tag{30}$$

2.4.3. The Korteweg-de Vries Equations

The KdV solution of the cnoidal wave is given by [35]:

$$C^2 = 1 + \frac{1}{k}(2 - k - 3\frac{E}{K}), \tag{31}$$

$$\eta = \frac{H}{k}(1 - k - \frac{E}{K}) + HC_n^2, \tag{32}$$

$$u_1 = (\eta - \eta^2 + \frac{1}{2}(\frac{1}{3} - (1 + x_2)^2)\frac{\partial^2 \eta}{\partial x_1^2})C, \tag{33}$$

$$u_2 = -(1 + x_2)((1 - 2\eta)\frac{\partial \eta}{\partial x_1} + \frac{1}{6}(1 - (1 + x_2)^2)\frac{\partial^3 \eta}{\partial x_1^3})C. \tag{34}$$

2.5. The Numerical Tank

A numerical tank is created in this study, in which solitary and cnoidal waves of different theories can be generated. Inside the domain, the fluid is governed by the NS equations. The computational domain of the numerical tank used in this study is 11.84 m long and 0.21 m deep, as shown in Figure 1. The wave generation and absorption zones in this study are shown in Figure 1, follow the same principle as those given by [36], within the open source computational fluid dynamics package, OpenFOAM. Waves are generated in a zone on the left of the tank. On the right-hand side of the domain, a relaxation zone is used to minimize the wave reflection back into the domain. The generation zone is set from $x_1 = -2$ m to $x_1 = 0$ and the relaxation zone is located at $x_1 = 7.84$ m to $x_1 = 9.84$ m. There are two wave gauges, GI located at the first node outside of the relaxation zone at $x_1 = 0$, and GII located at $x_1 - 2.62$ m from the end of the relaxation zone. Two pressure sensors, SI and SII, are placed on the tank bottom, at $x_2 = -1$, and two velocimeters, VI and VII, are placed at $x_2 = -0.3$. The horizontal location of the gauges are shown in Figure 1.

For the NS computations, two Intel Xeon E5-2697A v4 processors (16 cores, 40 M Cache, 3.00 GHz) are used. The maximum Courant Number is 0.25 and average Courant Number is 0.0086. All the cases are performed in 2D. The mesh sizes are $\Delta x_1/h = 0.067$ and $\Delta x_2/h = 0.167$, following the grid convergence study of [27].

We also use a tank that utilizes the GN equations both at the wavemaker and inside the domain, see [37] for details of the theoretical tank of the GN equations. See [38–41] for some studies on nonlinear wave dynamics and wave-structure interaction utilizing GN numerical tanks. For internal wave solutions of the GN equations, see, e.g., [42].

3. Results and Discussion

The results, including the surface elevations, velocities and pressure fields of solitary and cnoidal waves of different theories, are presented in this section. The results are compared with laboratory measurements where available and also with the results of the GN equations, (GN-GN, where both the wave maker and the domain are governed by the GN theory). The steady-state results generated by different theories are discussed first, followed by the unsteady results obtained from the computational tank. All results are given in a dimensionless form using ρ, g and h as a dimensionally independent set.

3.1. Steady-State Solution

The surface elevation of solitary waves generated by the five equations listed in Table 1 are presented first, followed by discussion on the surface elevations, horizontal velocities, and vertical velocities of cnoidal waves generated by the GN equations, the KP equations and the KdV equations.

3.1.1. Solitary Wave

The profiles of solitary waves with $A = 0.4$ generated by the Boussinesq equations, Laitone's 1st equations, Laitone's 2nd equations, the GN equations, and the KdV equations are shown in Figure 2.

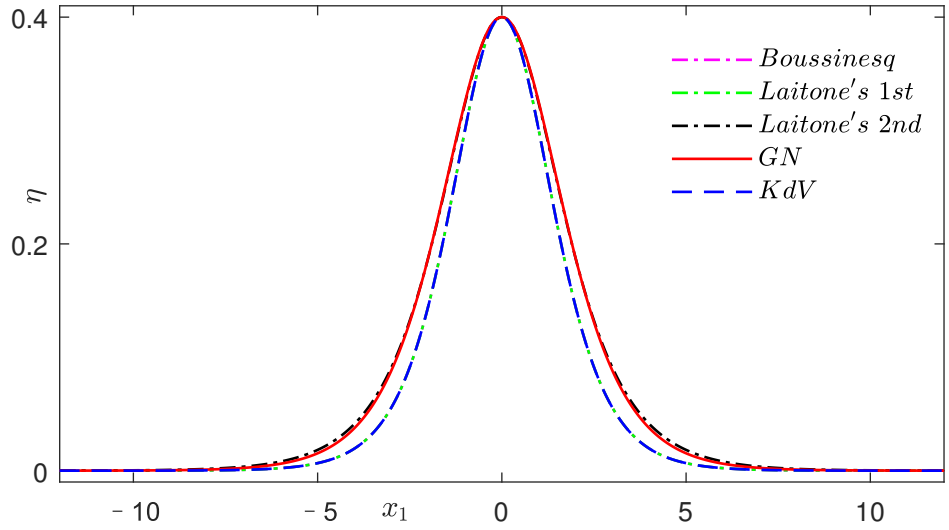

Figure 2. Comparisons of steady-state surface elevations of a solitary wave with $A = 0.4$, generated by various theories.

In Figure 2, the surface elevation of the Boussinesq equations and Laitone's 1st equations are covered by that of the KdV equations, as they share the same equation for η. The GN solution is wider, and that of Laitone's 2st theory is the widest.

In these cases, the theoretical wave speeds of the Boussinesq equations ($C = 1.1832$), the KdV equations ($C = 1.1832$), and the GN equations ($C = 1.1832$) are the same, followed by that of Laitone's 1st equations ($C = 1.2000$) is the fastest, and that of Laitone's 2nd equations ($C = 1.1760$) is the slowest.

3.1.2. Cnoidal Wave

The theoretical cnoidal wave surface elevation and velocity field, for $\lambda = 29.5$ and $H = 0.156,\ 0.311$, generated by the GN equations and the KP equations are shown in Figures 3–5, where λ is the wave length.

Figures 3–5 show that the results of the three equations are almost on top of each other, except there are small differences between the peak of the results. The peak of the surface elevation, horizontal and vertical velocities of the three equations are listed in Tables 2 and 3, together with the ratio, $R = \frac{\theta_M - \theta_{GN}}{\theta_{GN}} \times 100\%$, where θ is an arbitrary variable (η, u_1 or u_2), and M refers to different models.

Table 2. Comparisons of the peak values of the surface elevation, horizontal and vertical velocities of cnoidal wave ($H = 0.156$) of the GN equations and the KP equations.

	η	u_1	u_2
GN	0.1251	0.1145	0.0252
KP	0.1251	0.1219	0.0250
R	0.00%	6.46%	−0.79%
KdV	0.1251	0.1162	0.0247
R	0.00%	1.48%	−1.98%

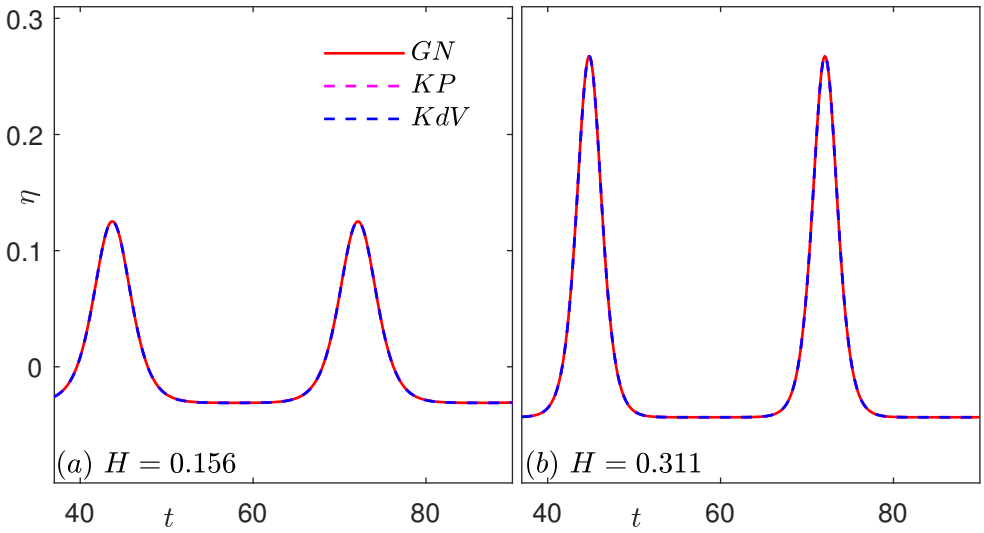

Figure 3. Comparisons of steady-state surface elevation of cnoidal waves generated by various theories. $\lambda = 29.6$.

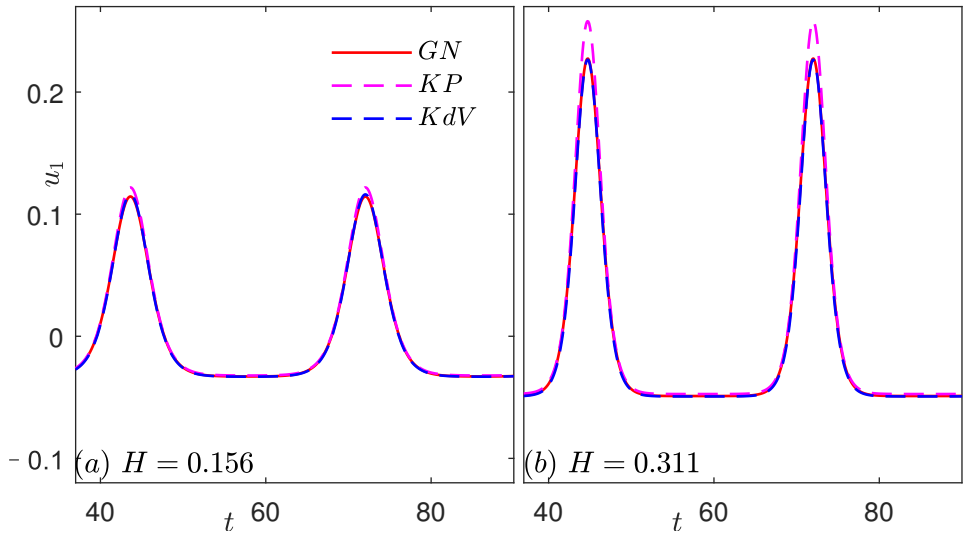

Figure 4. Comparisons of steady-state horizontal particle velocity of cnoidal waves generated by various theories. $\lambda = 29.6$.

Table 3. Comparisons of the peak values of the surface elevation, horizontal and vertical velocities of cnoidal wave ($H = 0.311$) of the GN equations and the KP equations.

	η	u_1	u_2
GN	0.2675	0.2273	0.0618
KP	0.2675	0.2580	0.0635
R	0.00%	13.51%	2.75%
KdV	0.2674	0.2265	0.0603
R	−0.04%	−0.35%	−2.43%

Shown in Figure 3, the peak values of the surface elevation of the three theories are the same, except that of the KdV equations with $H = 0.311$, which is 0.04% less than that of the other two equations. The same results are found for the vertical velocity, where the peak values are almost the same. The peak value of the horizontal velocity of the KP theory is significantly larger, where R is 6.46% and 13.51% for the two cases, than that of the other two theories.

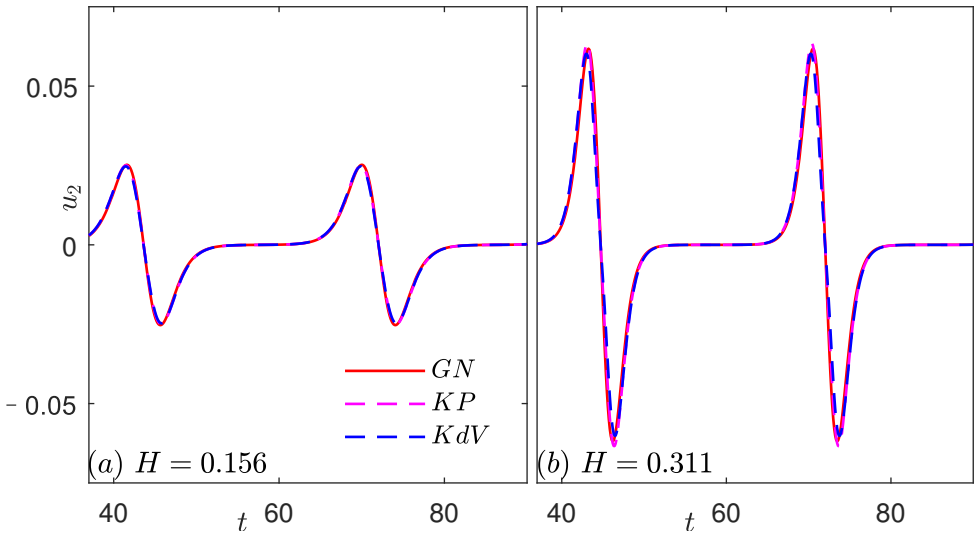

Figure 5. Comparisons of steady-state vertical particle velocity of cnoidal waves generated by various theories. $\lambda = 29.6$.

4. Unsteady Results

In this section, the propagation of solitary and cnoidal waves generated by a wave maker (using different theories) over a flat seafloor is studied. The wave maker is placed at $x_1 = 0$. In all cases, waves are generated by wave makers using different theories, and enter the domain governed by the NS equations. We also consider waves generated by the GN theory, entering a domain also governed by the GN equations. These combinations are listed in Table 4. The results for solitary waves are shown first, followed by the cnoidal wave results.

Table 4. List of the combination of wave makers and domain equations of the unsteady cases considered in this study.

Case	Wave Maker Theory	Domain Governing Equations	Type of Waves
KdV-NS	KdV	NS	solitary & cnoidal
KP-NS	KP	NS	cnoidal
GN-NS	GN	NS	solitary & cnoidal
GN-GN	GN	GN	solitary & cnoidal

4.1. Solitary Wave

Ref. [21] conducted laboratory experiments on the generation of solitary waves. They report the surface elevations of four cases with the same water depth $h = 0.114$ m. In all the cases presented in this subsection for cnoidal waves, water depth is fixed at $h = 0.114$ m. These four cases are listed in Table 5. Waves are measured in the wave flume in the absence of any obstruction by GII, located at $x_1 = 2.62$ m. These laboratory measurements are used for comparison here.

Table 5. Solitary wave cases considered in this study.

Case	A
1	0.192
2	0.301
3	0.408
4	0.525

Snapshots at $t = 0$ and surface elevations gathered by the GII of solitary waves are compared between GN-NS, KdV-NS, GN-GN, and laboratory experiments of [21], and are shown in Figures 6–9.

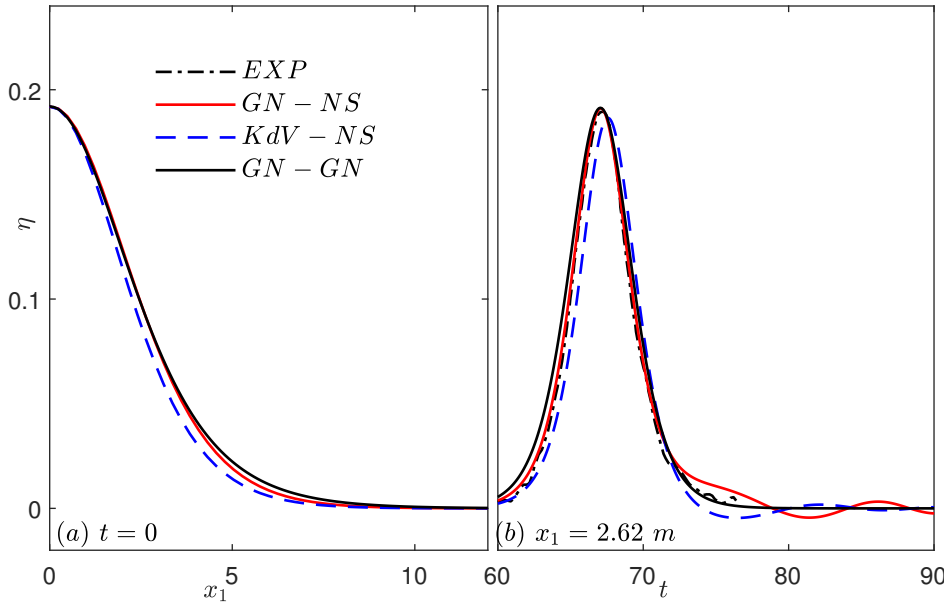

Figure 6. Comparisons of surface elevations of a solitary wave with $A = 0.192$, generated by the KdV and GN equations, propagating in domains of the NS and GN equations.

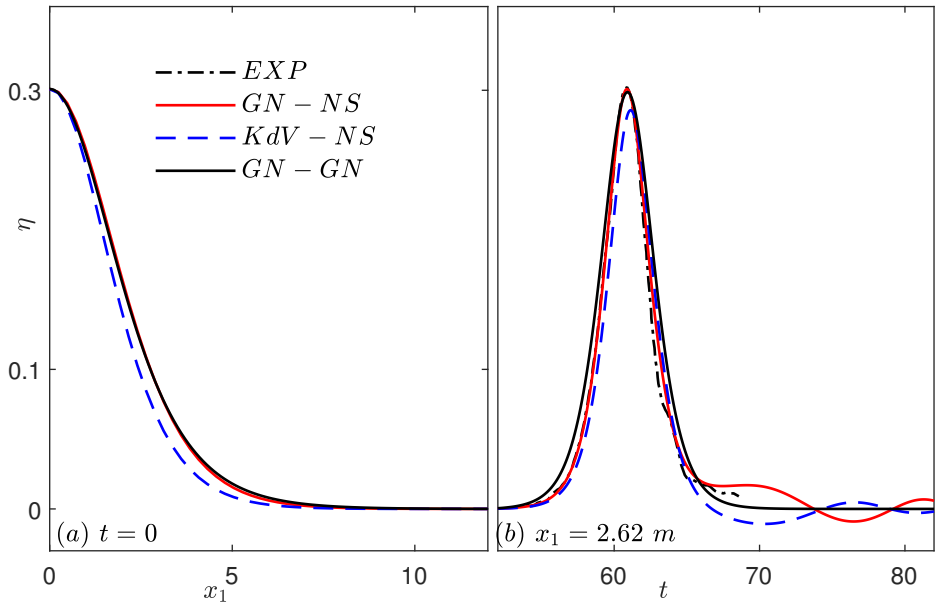

Figure 7. Comparisons of surface elevations of a solitary wave with $A = 0.301$, generated by the KdV and GN equations, propagating in domains of the NS and GN equations.

At $t = 0$, the surface elevations of GN-NS and GN-GN are almost identical (as expected), and the KdV-NS solitary wave is slimmer, see sub-figure (a) of Figures 6–9.

Table 6 shows the comparisons between the steady-state propagation speeds of solitary waves calculated by the equations listed in the table and unsteady ones measured from Figure 8 ($A = 0.4$). The wave speeds calculated by Laitone's 1st theory are the fastest, followed by those of the Boussinesq theory and the GN analytical solution, whose wave speeds are equal to each other. After these are the GN-GN, GN-NS and Laitone's 2nd theory. When compared to the other models, the KdV-NS predicts the slowest wave propagation.

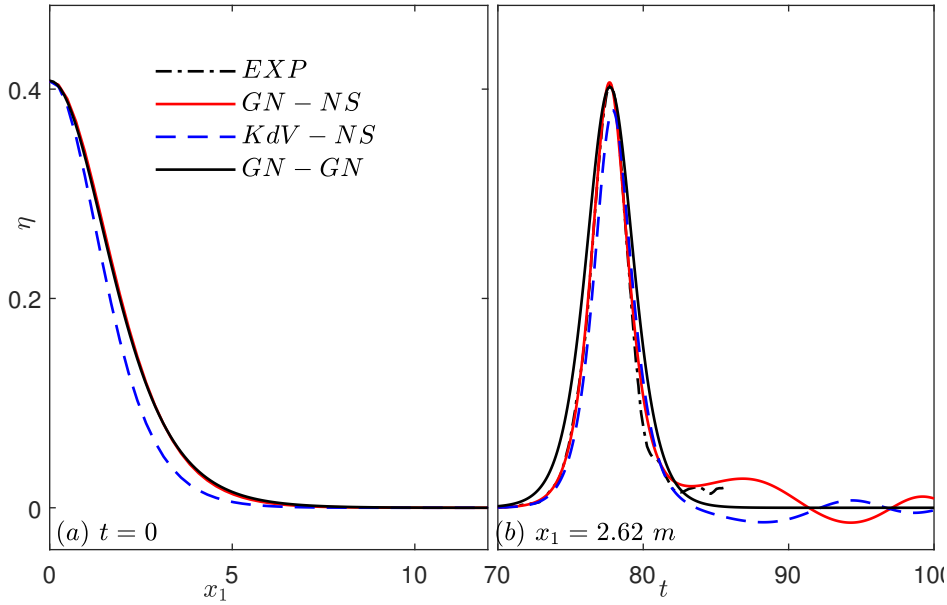

Figure 8. Comparisons of surface elevations of a solitary wave with $A = 0.408$, generated by the KdV and GN equations, propagating in domains of the NS and GN equations.

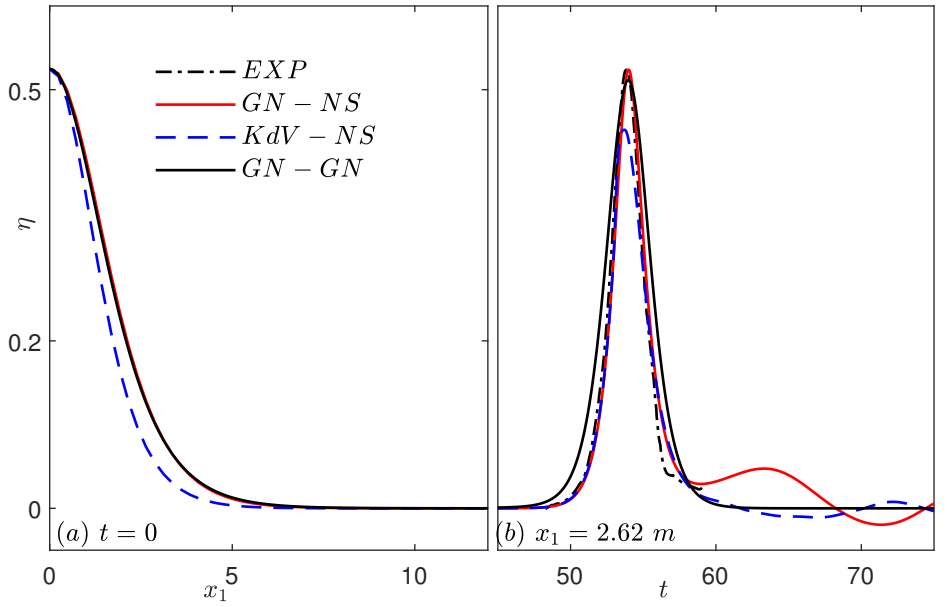

Figure 9. Comparisons of surface elevations of a solitary wave with $A = 0.525$, generated by the KdV and GN equations, propagating in domains of the NS and GN equations.

For the surface elevations recorded at x_1 = 2.62 m, the peak value of the GN-GN and the GN-NS drops slightly from the initial amplitude and are in good agreement with the laboratory experimental data of [21], while that of the KdV-NS drops more remarkably and is smaller than the laboratory measurements, particularly where the wave amplitude is larger, shown in sub-figures (b) of Figures 6–9. It shows the solitary wave generated by the GN equations are more stable than that of the KdV equations, especially in the cases of larger wave amplitudes.

Table 6. The analytical and numerical wave speeds of various theories ($A = 0.408$).

		Analytical	Value of C
Steady-state	Boussinesq Theory	$\sqrt{1+A}$	1.1832
	Laitone's 1st Theory	$\sqrt{1+A/2}$	1.2000
	Laitone's 2st Theory	$\sqrt{1+A/2-3A^2/20}$	1.1760
	GN Theory	$\sqrt{1+A}$	1.1832
	KdV equations	$\sqrt{1+A}$	1.1832
Unsteady	KdV-NS		1.1767
	GN-NS		1.1769
	GN-GN		1.1769

4.2. Cnoidal Wave

Ref. [43] conducted laboratory experiments on the generation of cnoidal waves in a tank with a flat floor. They report the surface elevations of cnoidal waves at water depth $h = 0.071$ m. In all the cases presented in this subsection for cnoidal waves, the water depth is fixed at $h = 0.071$ m. Details of two cases are listed in Table 7 used here for comparison. Waves are measured in the wave flume in the absence of any obstruction by only one gauge located at 2.62 m in the laboratory experiments.

Table 7. Cnoidal wave cases considered in this study.

Case	λ	H
1	29.6	0.156
2	29.6	0.311

The surface elevations recorded by the two wave gauges are presented in Figure 10. The results at $x_1 = 2.62$ m are compared between the experimental data of [43], and the numerical results of GN-NS, KP-NS, KdV-NS and GN-GN, in Figure 10.

Figure 10 shows that the results of the GN-GN model is the closest to the laboratory measurements. The wave speed of KP-NS is the fastest, followed by GN-NS, GN-GN, and KdV-NS.

The surface elevation differences between the experimental data and numerical results are presented in Table 8. In the table, $R = (\frac{P_M}{P} - 1) \times 100\%$, where P is the peak of the surface elevation in experiments and P_M is that of the equations. The average percentage difference ratios of the peak of the surface elevation of GN-NS (3.99%) and KdV-NS (4.36%) are close to each other, while that of KP-NS (5.71%) is the largest, and that of GN-GN (3.03%) is the smallest.

Table 8. The percentage differences between the peak of the surface elevation of cnoidal waves of different models and the laboratory measurements of [43]. $\lambda = 29.6$.

Case	$H = 0.156$	$H = 0.311$
Experiments	0.132	0.262
GN-NS	0.123	0.259
R	−6.82%	−1.15%
KP-NS	0.126	0.280
R	−4.55%	6.87%
KdV-NS	0.123	0.257
R	−6.82%	−1.90%
GN-GN	0.125	0.264
R	−5.30%	0.76%

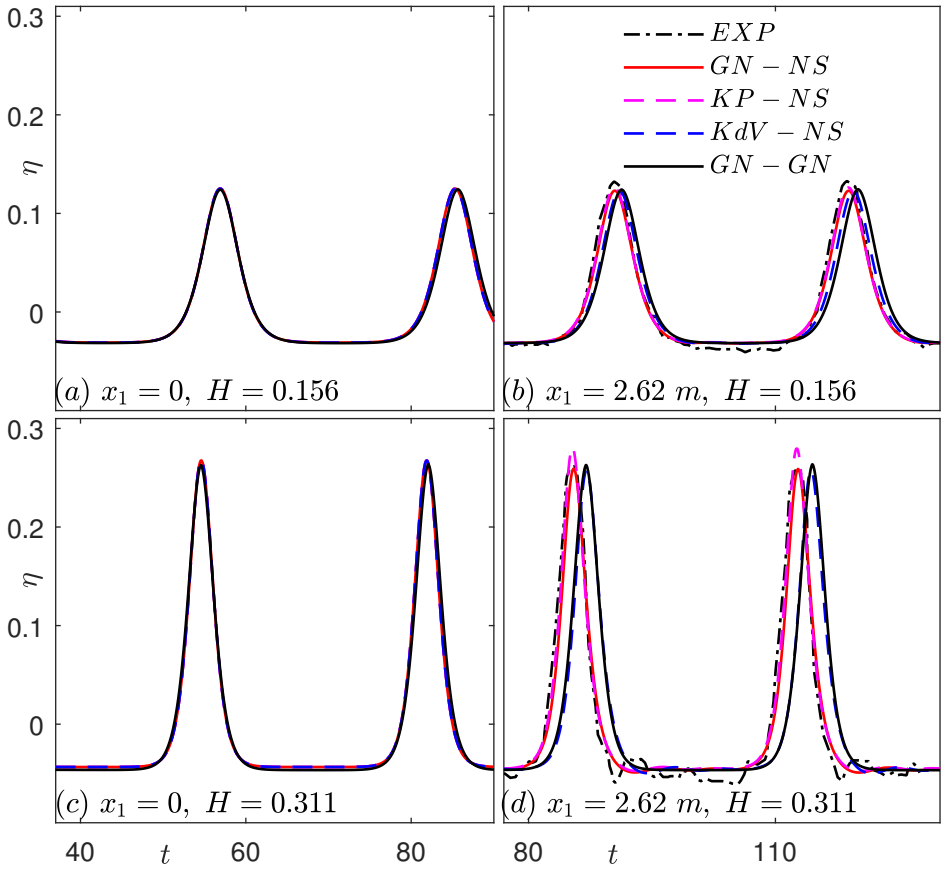

Figure 10. Comparisons of surface elevation of cnoidal waves of GN-NS, KP-NS, KdV-NS and GN-GN and the laboratory measurements of [43]. $\lambda = 29.6$.

Comparisons of pressures, horizontal and vertical velocities of the GN-NS, KP-NS, KdV-NS, and GN-GN models, recorded at pressure sensors, SI and SII, velocimeters, VI and VII, under GI and GII, respectively, of the two cases are presented in Figures 11, 12 and 13, respectively. In the absence of laboratory measurements of the pressure and velocity, and given that the surface elevations of the GN-GN is the closest to the laboratory experimental data, the GN-GN model is used as a benchmark and differences between the results of the models, $R = \frac{\theta - \theta_{GNGN}}{\theta_{GNGN}}$, are presented in Tables 9–11.

Table 9. The differences between the peak pressure of cnoidal waves generated by various theories.

Case	$H = 0.156$	$H = 0.311$
GN-GN	1.124	1.263
GN-NS	1.100	1.201
R	−2.14%	−4.91%
KP-NS	1.108	1.216
R	−1.42%	−3.72%
KdV-NS	1.105	1.200
R	−1.69%	−4.99%

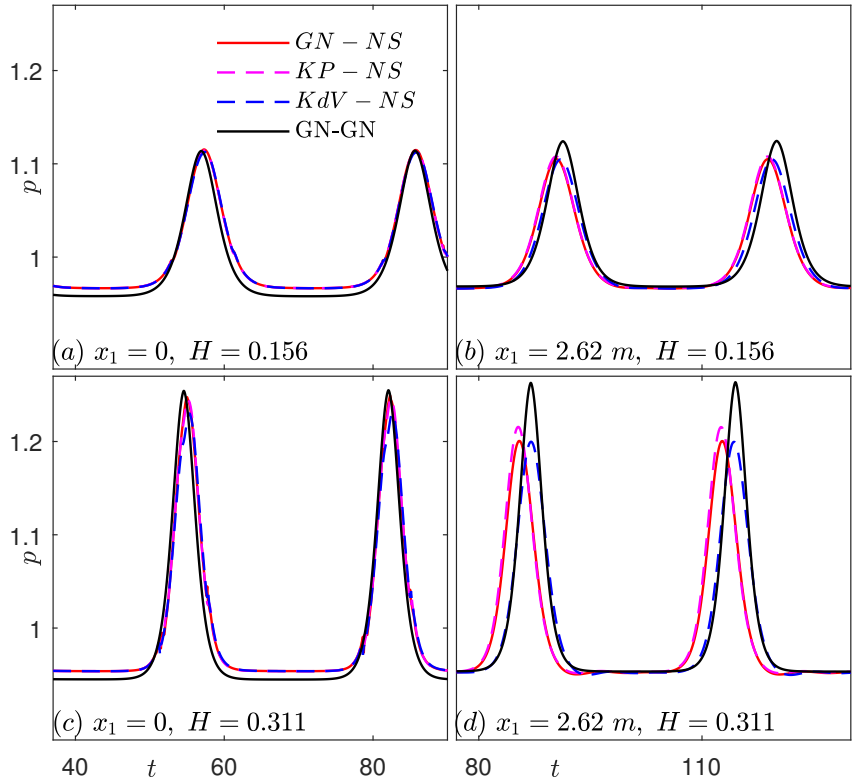

Figure 11. Comparisons of pressure of cnoidal waves of various theories, propagating in domain of the NS and GN equations. $\lambda = 29.6$.

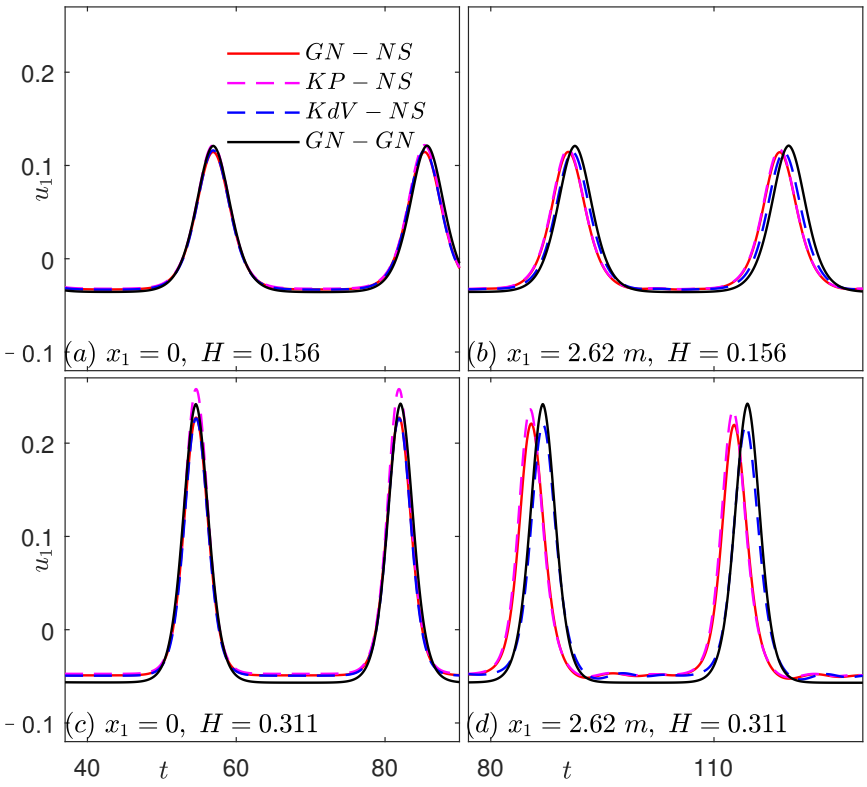

Figure 12. Comparisons of horizontal particle velocity of cnoidal waves generated by various theories, propagating in domain of the NS equations. $\lambda = 29.6$.

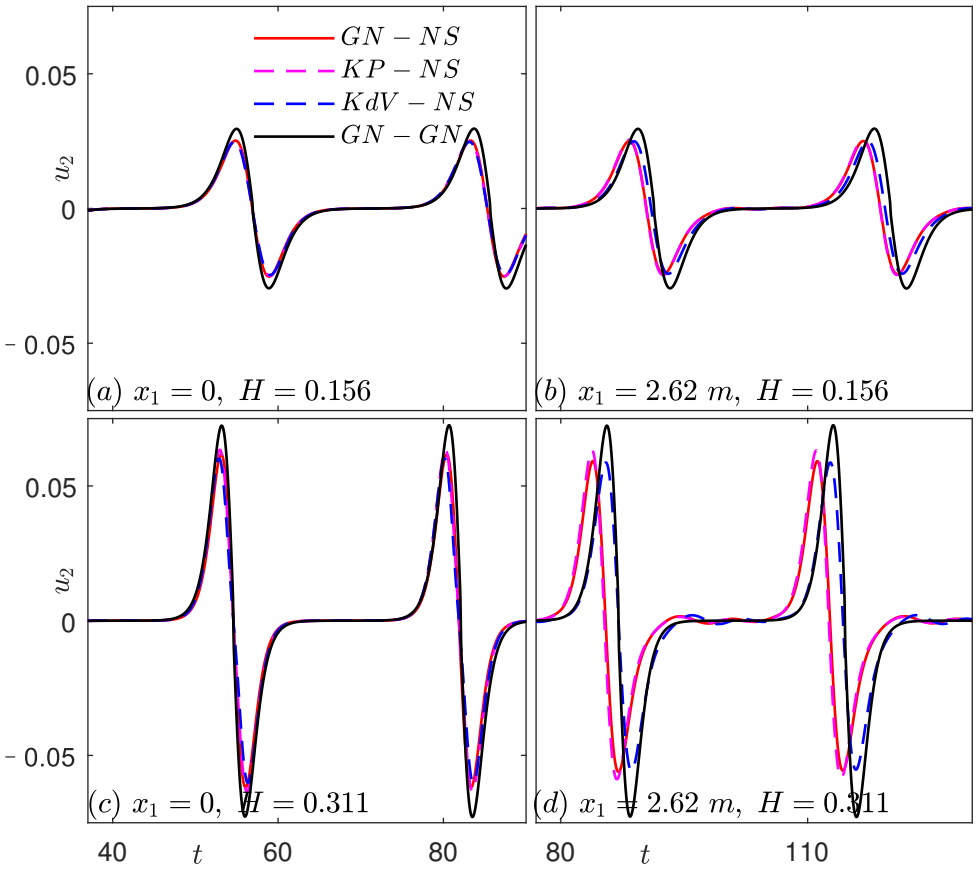

Figure 13. Comparisons of vertical particle velocity of cnoidal waves generated by various theories, propagating in domain of the NS equations. $\lambda = 29.6$.

Table 10. The differences between the peak horizontal velocity of cnoidal waves generated by various theories.

Case	$H = 0.156$	$H = 0.311$
GN-GN	0.121	0.242
GN-NS	0.114	0.220
R	−5.79%	−9.09%
KP-NS	0.117	0.235
R	−3.31%	−2.89%
KdV-NS	0.114	0.219
R	−5.79%	−9.50%

Table 11. The differences between the peak vertical velocity of cnoidal waves generated by various theories.

Case	$H = 0.156$	$H = 0.311$
GN-GN	0.0296	0.0726
GN-NS	0.0250	0.0592
R	−15.54%	−18.46%
KP-NS	0.0255	0.0632
R	−6.93%	−12.95%
KdV-NS	0.0249	0.0588
R	−15.88%	−19.00%

Figures 11–13 and Tables 9–11 show that p, u_1, u_2 of KP-NS are closer to that of GN-GN, while that of the GN-NS and KdV-NS are close to each other and slightly smaller than that of KP-NS.

We recall that in the Level I GN equations, we assume linear distributions of the vertical velocity. It is interesting to compare the results of GN-GN model with that of GN-NS and KP-NS to find out how close the assumption is to the computational results. Distribution of the horizontal and vertical velocity along the vertical direction at $x_1 = 0$ and $x_1 = 2.62$ m of the two cases are shown in Figures 14–17.

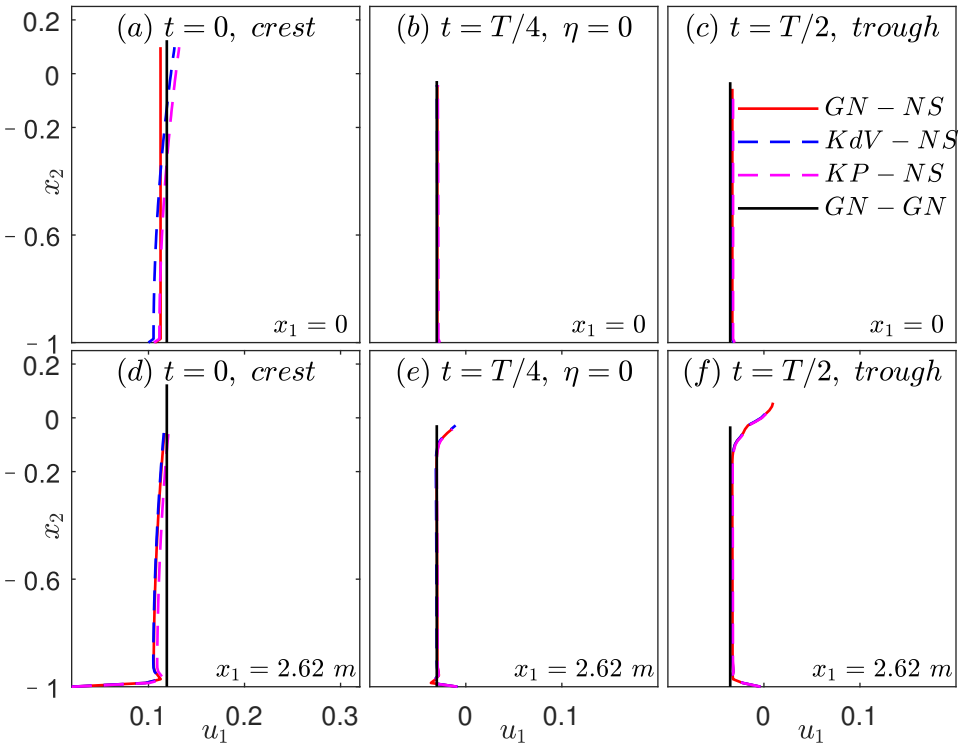

Figure 14. Comparisons of horizontal velocity distribution of cnoidal waves of theories, propagating in domains of the NS and GN equations in Case 1. $H = 0.156$, $\lambda = 29.6$.

For horizontal velocity distribution of cnoidal wave, GN-GN shows constant velocity along the vertical direction and this agrees with Equation (27). Although the horizontal velocity of GN-NS is constant at $x_1 = 0$, which is the same as GN-GN, the velocity becomes closer to that of KP-NS and KdV-NS as the wave propagates in the NS domain (at $x_1 = 2.62$ m). At $x_2 = 2.62$ m, the horizontal velocity of the cnoidal wave propagating in the NS domain shows a slight difference with that of GN-GN near the tank bottom and free surface. This is due to the effect of viscosity and the atmospheric boundary effects. Away from these boundaries, the horizontal velocities of the GN-NS, KP-NS and KdV-NS are constant and very close to that of the GN-GN model.

For vertical velocity distribution of cnoidal wave, that of GN-GN, GN-NS, KP-NS, and KdV-NS are almost linear along the vertical direction (agree with Equation (28) for the GN-GN model). Nonlinear distributions are found at $t = 0$, where the distributions under the crest is observed, see sub-figs (a) and (d) of Figures 16 and 17.

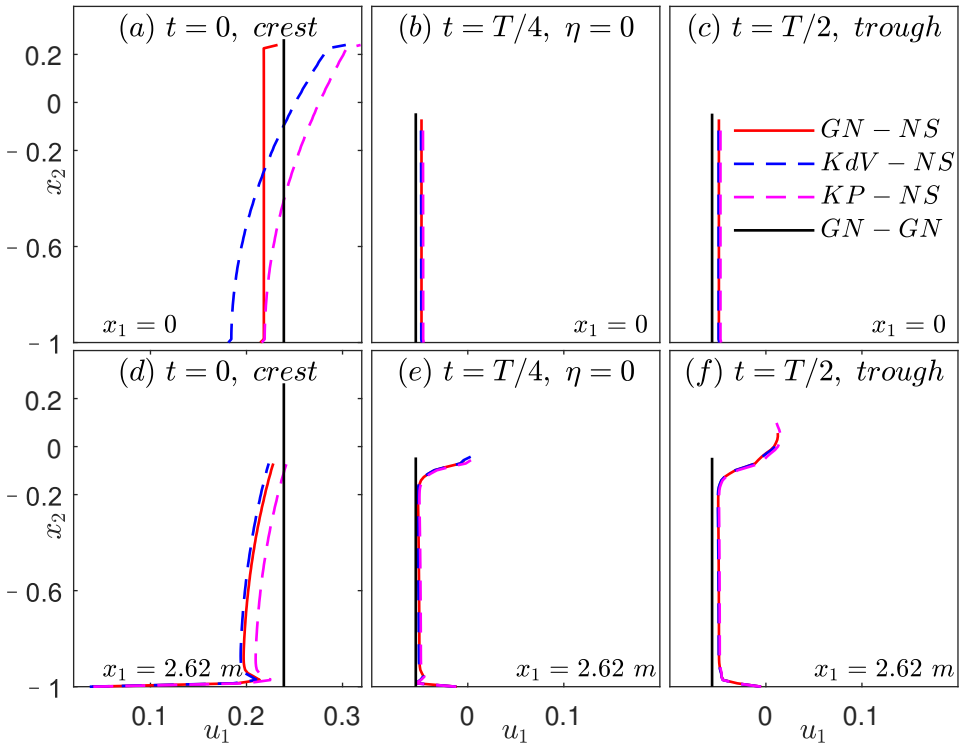

Figure 15. Comparisons of horizontal velocity distribution of cnoidal waves of theories, propagating in domains of the NS and GN equations in Case 2. $H = 0.311$, $\lambda = 29.6$.

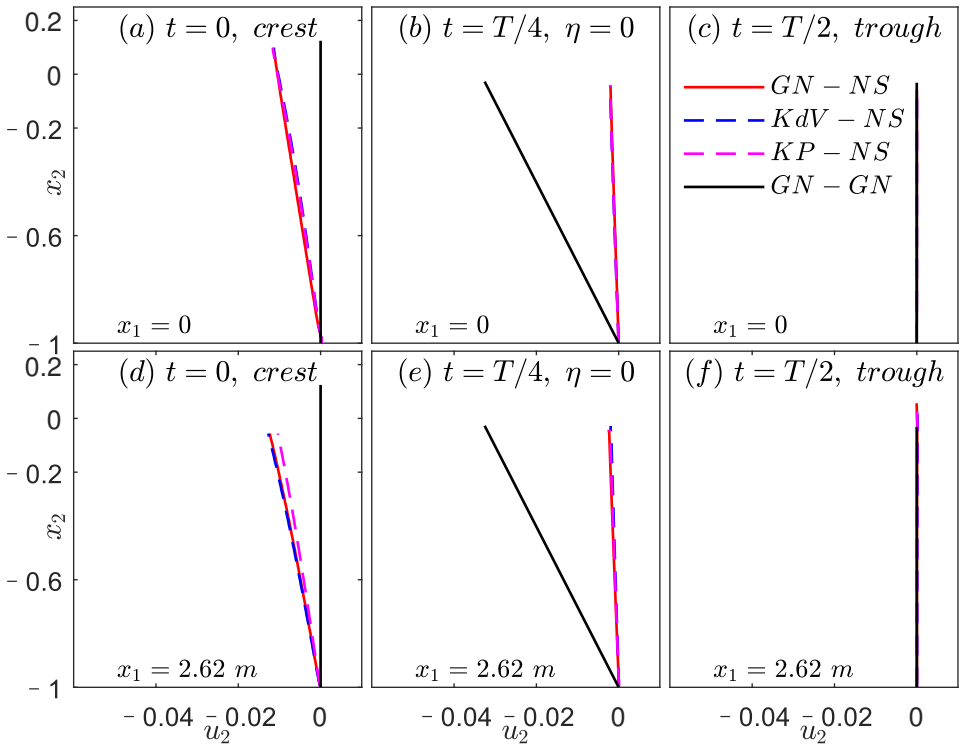

Figure 16. Comparisons of vertical velocity distribution of cnoidal waves of theories, propagating in domains of the NS and GN equations in Case 1. $H = 0.156$, $\lambda = 29.6$.

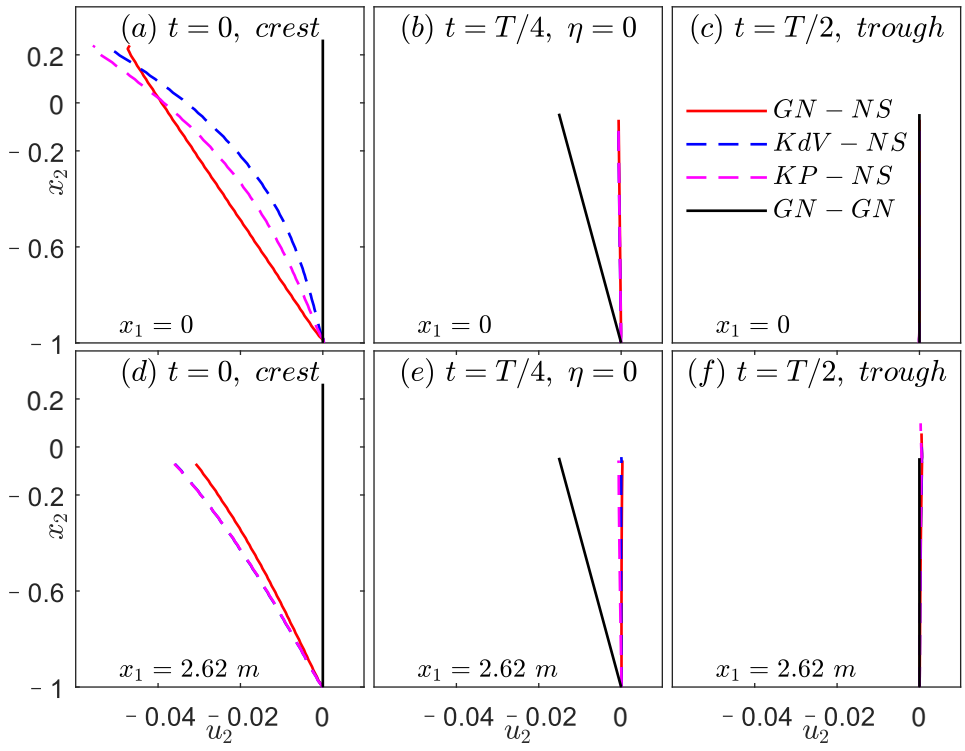

Figure 17. Comparisons of vertical velocity distribution of cnoidal waves of theories, propagating in domains of the NS and GN equations in Case 2. $H = 0.311$, $\lambda = 29.6$.

5. Concluding Remarks

The surface elevation, pressure and velocities of solitary and cnoidal waves generated by different theories are investigated. The stability and accuracy of the waves generated by different theories, propagating in a domain governed by the NS equations, are assessed. We have also considered waves generated by the GN equations, entering the domain of the GN equations.

For a steady-state solitary wave, the surface elevation of the wave generated by Laitone's 2nd is close to that of the GN equations, while those of the Boussinesq equations and Laitone's 1st are close to each other and slimmer than the previous two equations. The wave speed of Laitone's 1st equation is the largest, followed by the Boussinesq equations and the GN equations, and that of Laitone's 2nd is the slowest. Although the GN equations and the KdV equations share the same expression of wave speed for solitary waves, the speed of the wave in the GN-NS model is faster and closer to the theoretical values than that of KdV-NS, while that of GN-GN shows close agreement with the GN-NS model.

For the cnoidal wave, the surface elevation of the GN-GN model is closer to the experimental data, followed by KP-NS, GN-NS, and KdV-NS. Similar results are found for pressure, horizontal and vertical velocities. The wave speed of KP-NS is the fastest, GN-NS is the second, GN-GN is the third, and KdV-NS is the last. The main difference in the horizontal and vertical velocity distribution between GN-NS, KdV-NS, KP-NS, and GN-GN is found under the crest of the cnoidal wave, while the distributions are all the same when observed under the trough.

Overall, it is concluded that nonlinear waves generated by the GN equation are stable and show the least difference when compared with the laboratory measurements.

Author Contributions: Conceptualization, M.H. and R.C.E.; Methodology, M.H. and R.C.E.; Software, J.L., M.H. and R.C.E.; Validation, J.L. and M.H.; Formal analysis, J.L.; Investigation, J.L. and M.H.; Resources, M.H.; Writing—original draft, J.L.; Writing—review & editing, M.H. and R.C. E.;

Visualization, J.L.; Supervision, M.H. and R.C.E.; Project administration, M.H. All authors have read and agreed to the published version of the manuscript.

Funding: This research received no external funding.

Data Availability Statement: The data that support the findings of this study are available within the article.

Conflicts of Interest: The authors declare no conflict of interest.

References

1. Robison, J.; Scott, R.J. Report of the Committee on Waves. In Proceedings of the 7th Meeting of the British Association for the Advancement of Science, Liverpool, UK, September 1837; pp. 417–496.
2. Scott, R.J. Report on waves. In Proceedings of the Fourteenth Meeting of the British Association for the Advancement of Science, York, UK, September 1844; John Murray: London, UK, 1845; pp. 311–390.
3. Airy, G.B. *Tides and Waves, Section 192*; Encyclopedia Metropolitan: London, UK, 1845; Volume 5, pp. 241–396.
4. Boussinesq, M.J. Théorié de l'intumescence liquide, appelée onde solitaire ou de translation, se propageant dans un canal rectangulaire. *Acad. Sci. Comptes Rendus* **1871**, *73*, 755–759.
5. Boussinesq, M.J. Théorié générale des mouvements qui sont propagés dans un canal rectangulaire horizontal. *Acad. Sci.* **1871**, *73*, 256–260.
6. Boussinesq, M.J. Théorié des ondes et des remous qui se propagent Ie long d'un canal rectangulaire horizontal. en communiquant au liquide contenu dans ce canal des vitesses sensiblement pareilles de la surface au fond. *J. MathéMatiques Pures Appliquées* **1872**, *17*, 55–108.
7. Boussinesq, M.J. Essai sur la théorié des eaux courantes. *Mémoires Présentés Divers Savants L'Académie Sci. (Séries 2)* **1877**, *23*, 1–680.
8. Rayleigh, L. On waves. *Philos. Mag.* **1876**, *1*, 257–259.
9. McCowan, J. VII. On the solitary wave. *London Edinburgh Dublin Philos. Mag. J. Sci.* **1891**, *32*, 45–58.
10. Korteweg, D.J.; de Vries, G. On the change of form of long waves advancing in a rectangular canal and on a new type of long stationary waves. *Philos. Mag.* **1895**, *39*, 422–443.
11. Keulegan, G.H.; Patterson, J.A. Mathematical Theory of Irrotational Translation Waves. *J. Res. Natl. Bur. Stand.* **1940**, *24*, 47–101.
12. Littman, W. On the existence of periodic waves near critical speed. *Commun. Pure Appl. Math.* **1957**, *10*, 241–269.
13. Friedrichs, K.O. On the Derivation of the Shallow Water Theory, Appendix to the Formation of Breakers and Bores by J. J. Stoker. *Commun. Pure Appl. Math.* **1948**, *1*, 81–85.
14. Laitone, E.V. The second approximation to cnoidal and solitary waves. *J. Fluid Mech.* **1960**, *9*, 430–444.
15. Batchelor, C.K.; Batchelor, G.K. *Cnoidal Waves over a Gently Sloping Bottom*; Series Paper No. 6; Institute of Hydrodynamics and Hydraulic Engineering, Technical University of Denmark: Lyngby, Denmark, 1974.
16. Green, A.E.; Naghdi, P.M. A derivation of equations for wave propagation in water of variable depth. *J. Fluid Mech.* **1976**, *78*, 237–246.
17. Green, A.E.; Naghdi, P.M. Directed fluid sheets. *Proc. R. Soc. Lond.* **1976**, *347*, 447–473.
18. Sun, X. Some Theoretical and Numerical Studies on Two-Dimensional Cnoidal-Wave-Diffraction Problems. Ph.D. Thesis, University of Hawaii, Honolulu, HI, USA, 1991.
19. Hayatdavoodi, M.; Ertekin, R.C.; Valentine, B.D. Solitary and cnoidal wave scattering by a submerged horizontal plate in shallow water. *AIP Adv.* **2017**, *7*, 065212.
20. Hayatdavoodi, M.; Ertekin, R.C. Diffraction and Refraction of Nonlinear Waves by the Green–Naghdi Equations. *J. Offshore Mech. Arct. Eng.* **2022**, *145*, 021201.
21. Seiffert, B.; Hayatdavoodi, M.; Ertekin, R.C. Experiments and computations of solitary-wave forces on a coastal-bridge deck. Part I: Flat plate. *Coast. Eng.* **2014**, *88*, 194–209.
22. Hayatdavoodi, M.; Seiffert, B.; Ertekin, R.C. Experiments and Computations of Solitary-Wave Forces on a Coastal-Bridge Deck. Part II: Deck with Girders. *Coast. Eng.* **2014**, *88*, 210–228.
23. Hayatdavoodi, M.; Ertekin, R.C. Nonlinear wave loads on a submerged deck by the Green–Naghdi equations. *J. Offshore Mech. Arct. Eng.* **2015**, *137*, 011102.
24. Hayatdavoodi, M.; Seiffert, B.; Ertekin, R.C. Experiments and calculations of cnoidal wave loads on a flat plate in shallow-water. *J. Ocean Eng. Mar. Energy* **2015**, *1*, 77–99.
25. Hallak, T.S.; Islam, H.; Mohapatra, S.C.; Soares, C.G. Comparing Numerical and Analytical Solutions of Solitary Water Waves Over Finite and Variable Depth. In Proceedings of the 40th International Conference on Ocean, Offshore and Arctic Engineering, Online, 21–30 June 2021; American Society of Mechanical Engineers: New York, NY, USA, 2021.
26. Hirt, C.W.; Nichols, B.D. Volume of fluid (VOF) method for the dynamics of free boundaries. *J. Comput. Phys.* **1981**, *39*, 201–225.
27. Hayatdavoodi, M.; Liu, J.; Ertekin, R.C. Bore Impact on Decks of Coastal Structures. *J. Waterw. Port Coastal Ocean Eng.* **2021**, *148*, 04021051.
28. Higuera, P.; Lara, J.L.; Losada, I.J. Realistic wave generation and active wave absorption for Navier–Stokes models: Application to OpenFOAM®. *Coast. Eng.* **2013**, *71*, 102–118.

29. Greenshields, C.J. *OpenFOAM User Guide, Version 6*; OpenFOAM Found. Ltd., London, UK,: 2018.
30. Green, A.E.; Naghdi, P.M. Water waves in a nonhomogeneous incompressible fluid. *J. Appl. Mech.* **1977**, *44*, 523–528.
31. Neill, D.R.; Hayatdavoodi, M.; Ertekin, R.C. On solitary wave diffraction by multiple, in-line vertical cylinders. *Nonlinear Dyn.* **2018**, *91*, 975–994.
32. Hayatdavoodi, M.; Neill, D.R.; Ertekin, R.C. On Nonlinear Wave Diffraction by Vertical Cylinders in Shallow Water. *Theor. Comput. Fluid Dyn.* **2018**, *32*, 561–591.
33. Zhao, B.B.; Ertekin, R.C.; Duan, W.Y.; Hayatdavoodi, M.H. On the steady solitary-wave solution of the Green-Naghdi equations of different levels. *Wave Motion* **2014**, *51*, 1382–1395.
34. Zhao, B.B.; Duan, W.Y.; Ertekin, R.C.; Hayatdavoodi, M. High-level Green–Naghdi wave models for nonlinear wave transformation in three dimensions. *J. Ocean Eng. Mar. Energy* **2015**, *1*, 121–132.
35. Dingemans, M.W. Water wave propagation over uneven bottoms: Linear wave propagation. *Adv. Ser. Ocean Eng.* **1997**, *13*, 708–715.
36. Jacobsen, N.G.; Fuhrman, D.R.; Fredsøe, J. A Wave Generation Toolbox for the Open-Source CFD Library: OpenFoam®. *Int. J. Numer. Methods Fluids* **2012**, *70*, 1073–1088.
37. Ertekin, R.C.; Hayatdavoodi, M.; Kim, J.W. On some solitary and cnoidal wave diffraction solutions of the Green-Naghdi equations. *Appl. Ocean Res.* **2014**, *47*, 125–137.
38. Hayatdavoodi, M.; Ertekin, R.C. Wave Forces on a Submerged Horizontal Plate. Part I: Theory and Modelling. *J. Fluids Struct.* **2015**, *54*, 566–579.
39. Hayatdavoodi, M.; Ertekin, R.C. Wave Forces on a Submerged Horizontal Plate. Part II: Solitary and Cnoidal Waves. *J. Fluids Struct.* **2015**, *54*, 580–596.
40. Hayatdavoodi, M.; Treichel, K.; Ertekin, R.C. Parametric study of nonlinear wave loads on submerged decks in shallow water. *J. Fluids Struct.* **2019**, *86*, 266–289.
41. Hayatdavoodi, M.; Chen, Y.B.; Zhao, B.B.; Ertekin, R.C. Experiments and computations of wave-induced oscillations of submerged horizontal plates. *Phys. Fluids* **2023**, *35*, 017121.
42. Zhao, B.B.; Wang, Z.; Duan, W.; Ertekin, R.C.; Hayatdavoodi, M.; Zhang, T. Experimental and numerical studies on internal solitary waves with a free surface. *J. Fluid Mech.* **2020**, *899*, A17.
43. Seiffert, B.; Ertekin, R.C. Laboratory Generation of Solitary and Cnoidal Waves by the Green-Naghdi Equations. In Proceedings of the International Short Course and Conference on Applied Coastal Research, Florence, Italy, 28 September–2 October 2015.